Journal of
Applied and Computational Mechanics

Shahid Chamran
University of Ahvaz

Assessment of Drag Reduction Devices Mounted on a Simplified Tractor-Trailer Truck Model

Terrance Charles[ID], Zhiyin Yang[ID], Yiling Lu[ID]

School of Computing and Engineering, College of Science and Engineering, University of Derby, Derby, UK

Abstract. Aerodynamic drag reduction of tractor-trailer combination trucks is critically important to improve their fuel consumption which consequently results in lower emissions. One practical method to reduce aerodynamic drag of a truck is by mounting drag reduction devices on the truck. This paper presents a numerical study of turbulent flow over a simplified tractor-trailer truck with different drag reduction devices mounted on the truck using the Reynolds Averaged Navier-Stokes (RANS) approach to assess the effectiveness of those devices in drag reduction around the tractor-trailer gap region. Three cases with different drag reduction devices have been studied and significant drag reduction (above 30%) has been achieved for all three cases. Detailed analysis of the flow field has been carried out to understand drag reduction mechanisms, and it shows that no matter what drag reduction devices are deployed the drag reduction is mainly due to the reduced pressure on the front face of the trailer, and a small proportion of the drag reduction is due to the reduced turbulent kinetic energy in the gap region.

Keywords: Tractor-trailer combination truck, Aerodynamic drag, Drag reduction device, Numerical simulation.

1. Introduction

The aerodynamic drag of trucks is proportionally much higher in comparison with other ground vehicles due to their boxy shaped body [1] and hence drag reduction of a truck becomes very important since drag is directly linked to fuel consumption [2]. For a tractor-trailer combination truck travelling at highway cruising speeds, a 20% drag reduction would result in about 4% fuel saving [3]. Pressure drag accounts for a very high percentage of the total drag for the truck and is mainly generated in four areas: the front part of the tractor, the rear of the trailer, the undercarriage of the truck and the gap between the tractor and trailer [4]. The drag generated in the gap region between the tractor and trailer is about 20% of the overall pressure drag for a truck. Hence manipulating the flow field in the gap region through the deployment of various aerodynamics devices on the tractor and inside the gap region may result in aerodynamic drag reduction, which is the focus of this study.

Aerodynamic devices can be classified into two categories, a) Passive aerodynamic device: aerodynamic devices which do not make use of any energy to alter the flow characteristics which lead to drag reduction, b) Active aerodynamic device: devices which use energy to alter the flow characteristics which lead to drag reduction. By comparison passive aerodynamic devices are cost efficient, simple and yet effective and hence are more popular than active aerodynamic devices. The present study will focus on only passive aerodynamics devices.

One of the simplest, yet an effective passive aerodynamic drag reduction device used in the gap region is called Cross Vortex Trap Device (CVTD). CVTD consists of equally spaced vertical splitter plates which are mounted vertically on the front face of the trailer, aiming to stabilize the flow in the gap region. Charles *et al.* [5] carried out an in-depth numerical analysis on three different configurations of CVTD mounted on the front face of the trailer. The configurations included single, double and triple vortex trap layout. It was shown that the triple vortex trap layout was the most effective with nearly 15% drag reduction when compared against the baseline case.

Another simple and widely used passive aerodynamic device is the cab roof deflector which has been used not only on heavy trucks but also on pickup trucks, small trucks, and road trains. Cab roof deflector is used to guide the flow by reducing flow separation and turbulence along the upper part of the tractor, and especially to avoid direct flow impingement onto the front face of the trailer in tractor-trailer trucks [6].

Despite many previous studies on aerodynamic add-on devices developed to reduce drag within the gap region, there has been a lack of systematic studies to properly assess the effectiveness of those devices, especially on the combination of those devices. Therefore, it is still not fully clear how to configure these aerodynamic add-on devices to achieve maximum drag reduction within the gap region. The main focus of the present study is to assess the effectiveness of three drag reduction devices (cab roof deflector, side extender, CVTD) and their combination, shedding light on the drag reduction mechanisms of those devices, which could lead to better drag reduction device design in the future. The numerical approach employed is the RANS since other two main approaches, Large Eddy Simulation (LES) and Direct Numerical Simulation (DNS), are computationally very expensive and for practical engineering flow simulations [7], especially for optimization studies where a large number of

simulations is needed, the RANS approach is still the most feasible one at the moment and in the near future.

This paper is structured as follows: mathematical formulation, details of computational setup including, grid independent study results and justification of turbulence model selection are given in section 2. Numerical results, analysis and discussion are presented in section 3 and the concluding remarks are provided in section 4.

2. Governing Equations and Computational Setup

2.1 Governing Equations

The governing equations (Navier-Stokes equations) for fluid flow are derived from mass and momentum conservation laws. These equations are three dimensional and time dependent for a turbulent flow. In the present study, the RANS approach is employed and the RANS equations are obtained by time averaging the instantaneous governing equations. This averaging process leads to extra terms called Reynolds stresses which need to be modelled (approximated) by a turbulence model, otherwise the number of unknowns would be more than the number of equations.

The flow considered in the present study is isothermal (no heat transfer present) and incompressible (low velocity). The RANS equations for incompressible flow is briefly presented below since those equations are fairly standard and are available in many textbooks and publications [8 - 10].

Continuity equation:

$$\frac{\partial \bar{U}_i}{\partial x_i} = 0 \tag{1}$$

Momentum equation:

$$\frac{\partial \bar{U}_i \bar{U}_j}{\partial x_i} = -\frac{1}{\rho}\frac{\partial \bar{P}}{\partial x_i} + \frac{\partial}{\partial x_i}\left[\nu \frac{\partial \bar{U}_j}{\partial x_i}\right] - \frac{\partial \left(\overline{u_i' u_j'}\right)}{\partial x_i} \tag{2}$$

The term $\partial(\overline{u_i' u_j'})/\partial x_i$ in equation 2 is the Reynolds stress term and to model this term, turbulence modelling is required. Many turbulence models have been developed but there is not a consensus that which model is the best as their performances are flow dependent, and there is no evidence suggesting that one particular model performs better in many different flow situations than all other models. Hence three widely used and highly rated turbulence models, the realizable *k-ε*, SST *k-ω* and a Reynolds Stress Model (RSM), have been tried in the present study to check which one performs best in this kind of flow. There are a few different RSMs depending mainly on how to model the turbulent diffusive term and the pressure-strain term. The turbulent diffusive term is modeled based on the generalized gradient diffusion model of Daly and Harlow [11], and the pressure-strain term is modeled by a linear model proposed by Gibson and Launder [12] in the present study.

The governing equations are discretized using a finite volume method (2nd order upwind scheme) and solved numerically with a pressure-based approach since the flow is treated as incompressible. A commercial computer code, STAR CCM+, is used in the present study.
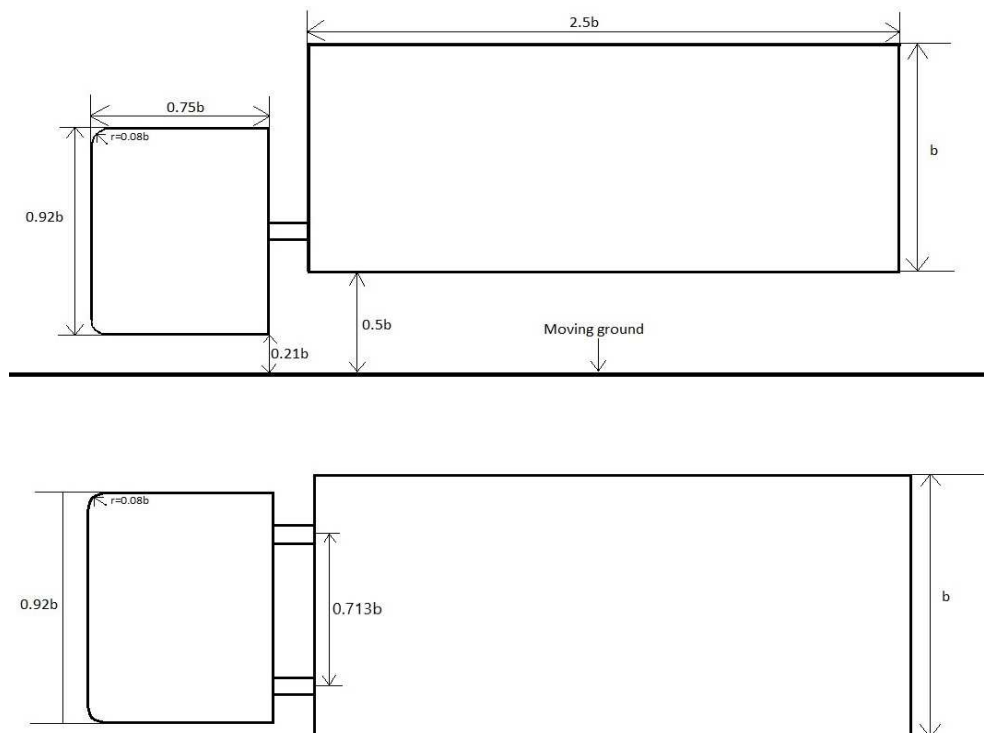

Fig. 1. Schematic of the tractor-trailer model.

2.2 Computational Setup

The baseline test case employed in the present study is based on a wind tunnel experiment by Allan [13]. A simplified tractor-trailer truck model, as shown in Fig. 1, was used in the experiment with a Reynolds number of 0.51×10^6 based on the inlet velocity and the height of the trailer. Two different models were used in the experiment [13]. The first model is a tractor with sharp leading edges and the second model is a tractor with curved leading edges. In the present study only the second model, a tractor with curved leading edges, has been considered. All the dimensions of the truck are shown in Fig. 1, which are measured relative to the trailer height and width, b = 0.305m. The gap ratio g/b is equal to 0.17 and the front edges of the tractor are curved at a radius of 0.08b.

The dimensions of the computational domain are selected to match those of the wind tunnel used in the experiment. Figures 2 and 3 show the side view and the front view of the computational domain.

A constant velocity of 24.4 m/s is specified at the inlet, which matches the value used in the experiments and a pressure outlet boundary condition is used at the outflow boundary. A no-slip wall boundary condition is applied to the top/side walls, and to all solid surfaces of the model. On the lower wall the velocity component in the streamwise direction is set equal to the inlet velocity, matching the moving ground condition in the experiment. There is no information available from the experiment about the inlet turbulence intensity and hence a representative low turbulence wind tunnel value of 0.1% has been used in the present study.
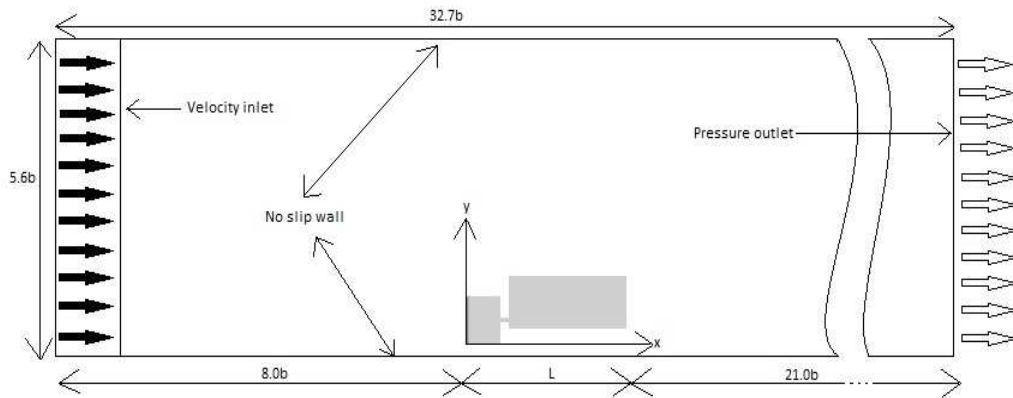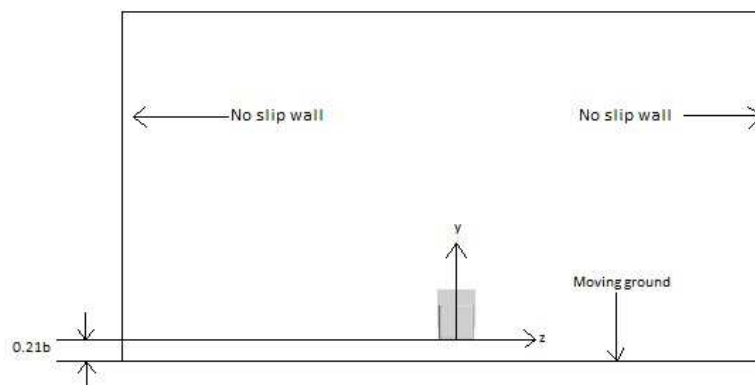

Fig. 2. Computational domain - side view.

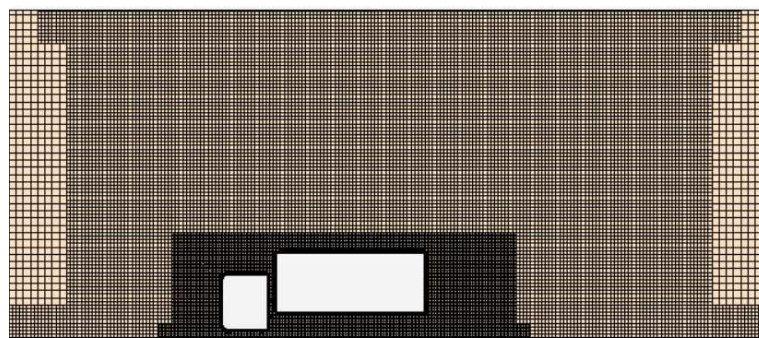**Fig. 3.** Computational domain - front view.

Fig. 4. Computational grid showing local mesh refinement.

2.3 Grid Independence Study

A grid independence study has been carried out to minimize numerical errors and reduce wasting computational resources. It has been found that significant discrepancies exist when using polyhedral mesh while more consistent results have been obtained when using a trimmed cell mesh. Trimmed cell mesh tends to provide an efficient and more robust higher quality grid for simple geometries, which is the case in the present study. Hence, a trimmed cell mesh has been employed in this present study. Furthermore, refining the mesh locally in certain flow regions is necessary to capture accurately the very complex nature of turbulent flow field generated in those regions due to flow separation and recirculation. A volumetric control has been applied to specific zones within the computational domain to achieve the required local mesh refinement as shown in Fig. 4.

Three different grids with trimmed cell mesh and local mesh refinement as discussed above have been used in this present study: a coarse grid with 4.0 million cells, a medium grid with 5.8 million cells and a fine grid with 8.1 million cells. Figures 5 and 6 show the predicted axial velocity profiles plotted against the vertical distance at two axial locations in the vertical symmetric plane behind the truck. It can be seen from the figures that the predicted results obtained from the coarse grid are considerably different from those obtained from the medium and fine grids, and the predicted results from the medium grid are much closer to the results from the fine grid. Furthermore, the predicted drag coefficient is 0.88 using the coarse grid, 0.81 using the medium grid and 0.82 using the fine mesh, which clearly demonstrates that the predicted drag coefficient using the medium grid is very close to the predicted drag coefficient using the fine mesh. Hence there is no need to refine the grid further and to make it computationally efficiently the medium grid has been used in the present study with the nearest wall y+ being kept close to 1 to avoid using a wall function.

2.4 Turbulence Model Selection

The predicted drag coefficients using the three turbulence models have been presented in Table 1 below and it can be seen that the SST k-ω model produces the closest drag coefficient to the measured value in this flow condition. Hence it has been selected in the present study.
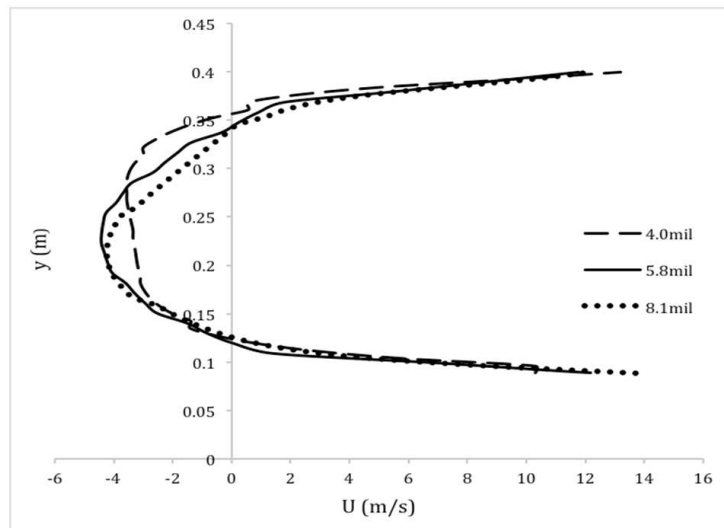

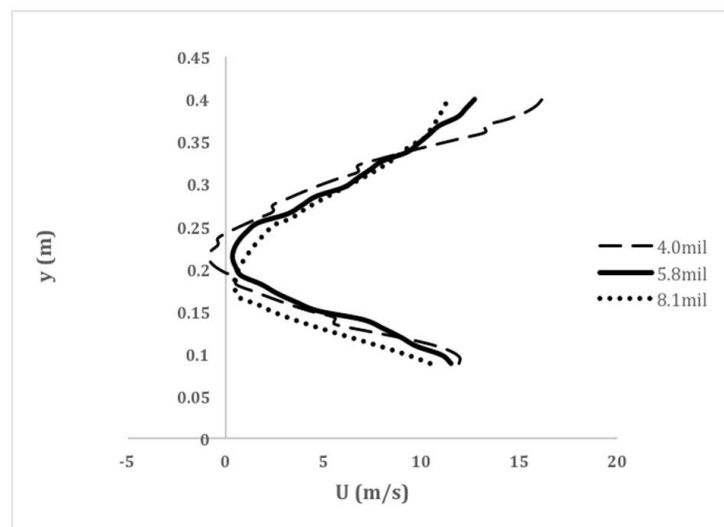**Fig. 5.** Axial velocity profiles at x = 1.13 m.

Fig. 6. Axial velocity profiles at x = 1.43m.

Table 1. Predicted and measured drag coefficients

	C_d	ΔC_d
Experiment [10]	0.77	
Realizable k-ε	0.862	11.95%
SST k-ω	0.809	5.06%
RSM	0.820	6.49%

Table 2. The predicted drag coefficients.

	Predicted	ΔC_d
Baseline case	0.809	
Case 1	0.534	34%
Case 2	0.496	38.7%
Case 3	0.487	39.8%

3. Results and Discussion

The computational approach used in the present study has been validated previously and comparison of the predictions against experimental data can be found elsewhere [4, 5]. The drag reduction devices discussed in this section are mounted to either the tractor or trailer as shown in Fig. 7. The following cases have been numerically simulated:

Baseline case: without any devices
Case 1: baseline case with roof deflector.
Case 2: baseline case with roof deflector and side extenders.
Case 3: similar to case 2 plus a CVTD mounted on the front face of the trailer.

3.1 Predicted Drag Coefficient

The drag reduction achieved by the three cases in comparison with the baseline case are presented in Table 2. It can be seen that a significant drag reduction has been achieved for all three cases. Even for case 1 with roof deflector alone a drag reduction of 34% is achieved, which is much better than the previous maximum drag reduction of about 15% with the best CVTD configuration (a triple vortex trap layout) mounted on the trailer front face [5]. This strongly suggests that devices mounted on the tractor are more effective in drag reduction than devices deployed in the gap region and flow field analysis below will explain the reason behind this. A further drag reduction of 4.7% is achieved in case 2 where a side extender is added on both sides of the tractor apart from the roof deflector. The maximum drag reduction of 39.8% is obtained in case 3 where all three devices (roof deflector, side extenders and a CVTD) are deployed. Detailed analysis will be presented below to reveal the drag reduction mechanisms for those cases.
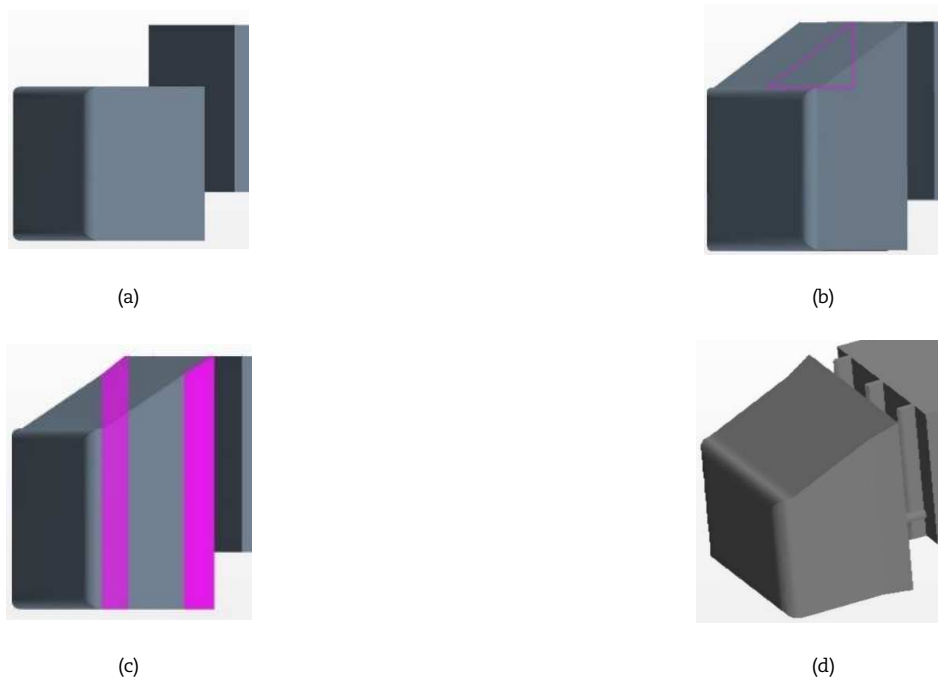

(a)

(b)

(c)

(d)

Fig. 1. Configurations of test cases. (a) Baseline case, (b) Case 1 (baseline is added with roof deflector), (c) Case 2 (case 1 is added with side-extender), (d) Case 3 (case 2 is further added with CVTD).

3.2 Flow field and surface pressure distribution

Figure 8 presents the predicted velocity vectors coloured by the velocity magnitude on the XY plane at z = 0 for the baseline case and case 1. It can be seen from Fig. 8a for the baseline case that a strong recirculation region exists on top surface of the tractor. A proportion of the flow above the tractor impinges directly on the top part of the front surface of the trailer before entering the gap region and the remaining flow passes the gap, moving on to the top surface of the trailer towards the trailing end of the truck. The flow entering the gap from the top moves towards the bottom of the gap and eventually goes out, mixing with the mainstream flow along the bottom of the trailer. For case 1 where a roof deflector is mounted on top of the tractor this big recirculation region on the top surface of the tractor disappears and the amount of flow entering the gap region is significantly reduced. In particular, the flow impingement directly on the top part of the front surface is eliminated completely as shown in Figure 8b, resulting in a significant reduction pressure on the front face of the trailer. This can be confirmed from Fig. 9 and Fig. 10 which show contours of pressure coefficient for the baseline case and case 1. It can be seen in Fig. 9 for the baseline case that two high pressure regions are clearly observable on the front face of the tractor and top part of the front face of the trailer, which is due to flow impingement directly on those two regions. However, the high-pressure region on top part of the front face of the trailer has disappeared completely for case 1 as shown in Fig. 10, leading to a significant pressure drag reduction.

It can be seen from Table 2 that the drag coefficient is further reduced in case 2 when the side extenders are used and this reduction can be explained from Fig. 11 which shows contours of pressure coefficient on the front face of the trailer for case 1 and case 2. For case 1 as shown in Fig. 11a that there are two small narrow vertical regions of high pressure near the lateral sides on the front face of the trailer. This is because the width of the tractor is less than the width of the trailer which results in flow impingement on those two small regions on the front face of the trailer. However, for case 2 the pressure in those two regions is reduced since the flow impingement on those areas has been eliminated due to the use of the side extenders, leading to further drag reduction.
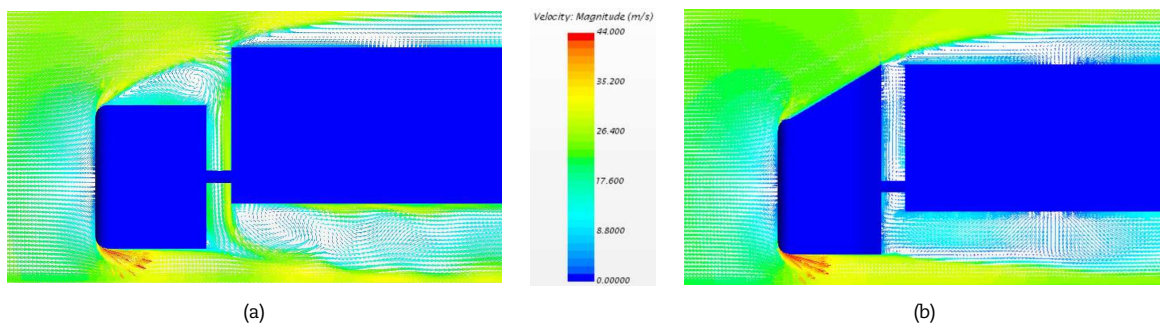

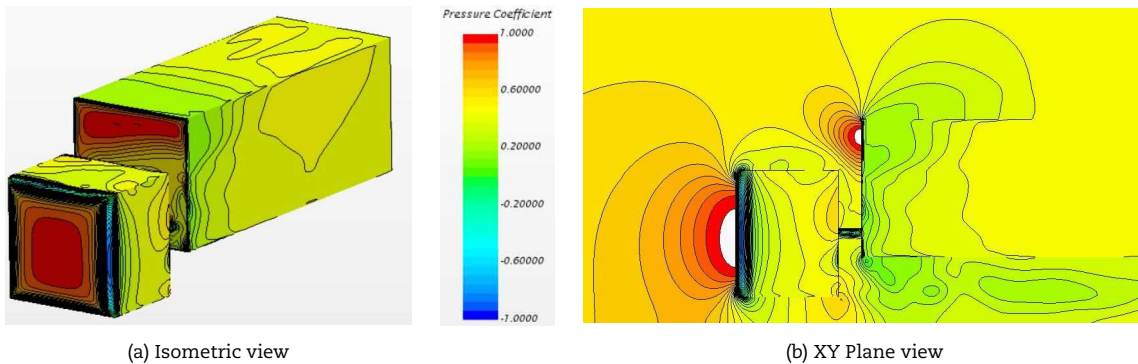**Fig. 8.** Velocity vectors on the XY plane at Z=0.

(a) Isometric view   (b) XY Plane view

Fig. 9. Pressure coefficient contours for the baseline case.

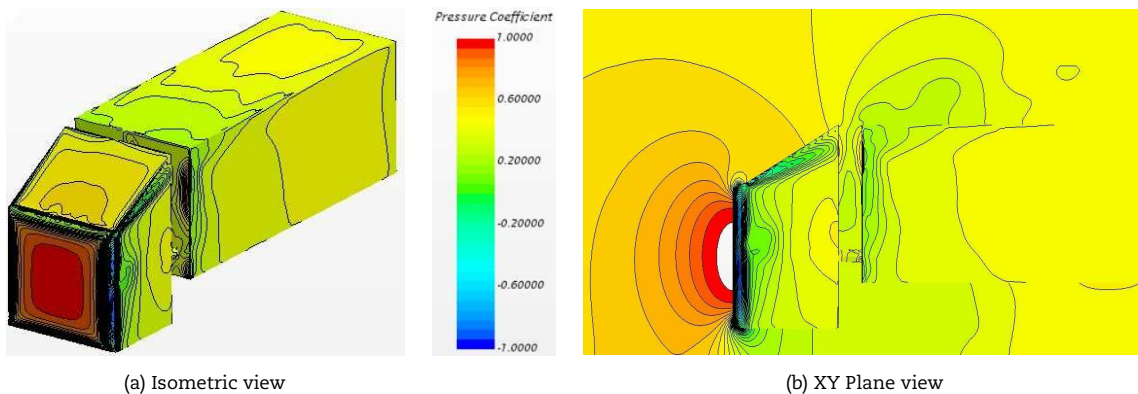(a) Isometric view   (b) XY Plane view

Fig. 10. Pressure coefficient contours for case 1.

Figure 12 presents a qualitative comparison of the predicted flow fields within the gap region on the XZ plane at y = 0.2 m and it can be seen that the deployment of devices alters the flow characteristics significantly. For the baseline case without any drag reduction device there is a strong interaction between the flow entering from top and the flow entering from lateral sides, resulting in a very turbulent flow field within the gap itself as shown in Fig. 12a. When the roof deflector is deployed in case 1, the amount of flow entering from the top is significantly reduced, leading to much weaker downwash and the flow field inside the gap is mainly due to the interaction between the inward turning flow along the lateral sides of the tractor as shown in Fig. 12b. With the addition of side extenders in case 2 the interaction between the inward turning flow along the lateral sides of the tractor becomes weaker due to less amount of flow entering from the lateral sides, and hence the flow is less turbulent as shown in Fig. 12c. For case 3, addition of the triple vortex trap device on the front face of the trailer stabilizes the vortices formed within the gap region and reduces the mixing of the flow further, resulting in less turbulence and hence leading a further drag reduction as shown in Fig. 12d. The reduction of turbulence level in the gap region can be further confirmed from Fig. 13 showing velocity vectors coloured by the velocity magnitude on the YZ plane in the gap at X=0.026m from the rear face of the tractor. It can be seen that the flow is still quite turbulent as shown in Fig. 13a when only the roof deflector is deployed in case 1 and with the addition of side extenders in case 2 the flow becomes much less turbulent as both the velocity magnitude and the vorticity decrease significantly as shown in Fig. 13b. When the triple vortex trap device is mounted on the front face of the trailer the flow becomes very smooth (more or less laminar flow) as shown in Fig. 13c.
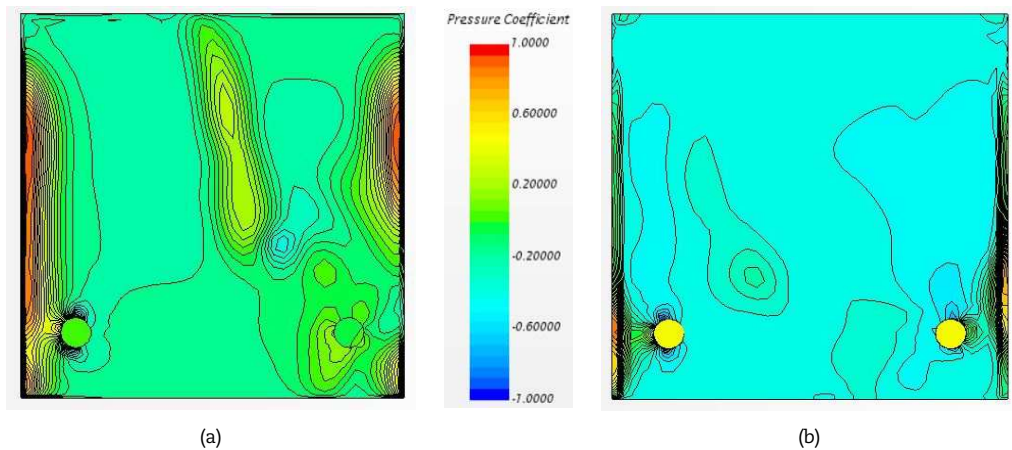

(a)   (b)

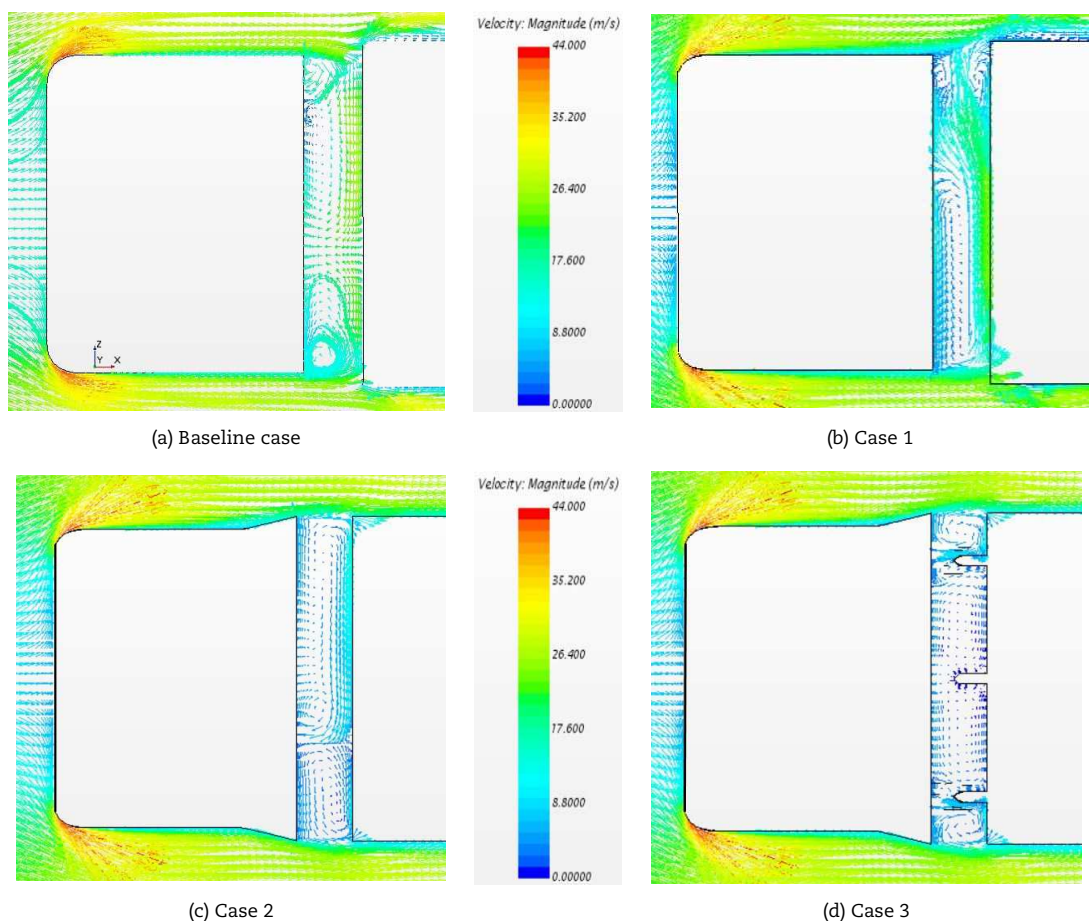**Fig. 11.** Pressure coefficient contours on the front face of the trailer, (a) case 1, (b) case 2.

(a) Baseline case   (b) Case 1

(c) Case 2   (d) Case 3

Fig. 12. Velocity vectors on the XZ plane at y = 0.20m.
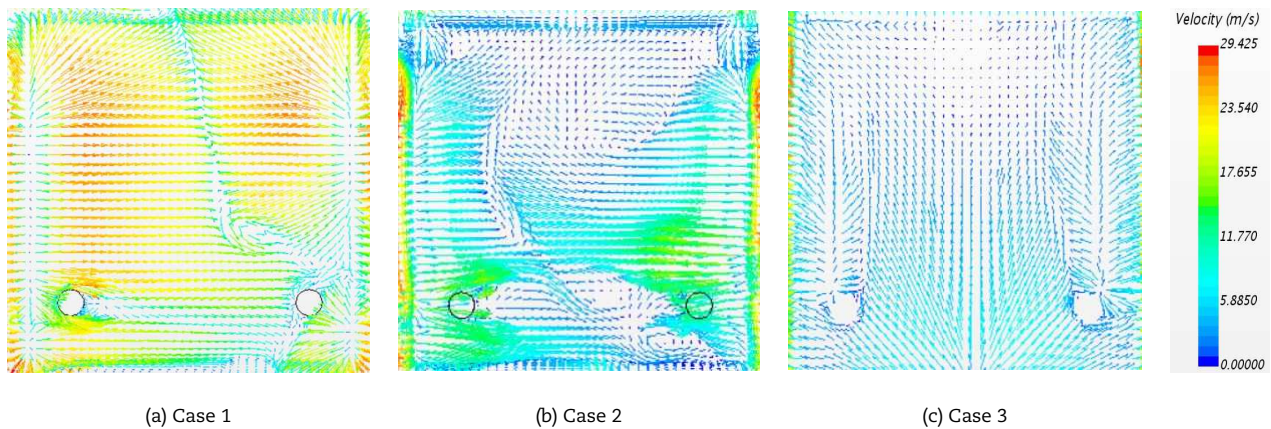
| (a) Case 1 | (b) Case 2 | (c) Case 3 |

Fig. 13. Velocity vectors on the YZ plane in the gap at x = 0.026m

4. Conclusion

A numerical study of turbulent flow around a simplified tractor-trailer truck model with three drag reduction devices (roof deflector, side extender and CVTD) has been carried out using a steady RANS approach to assess the effectiveness of those devices. Three turbulence models (realizable k-ε, SST k-ω and RSM) have been assessed for this kind of flow and the SST k-ω model performs best as the predicted drag coefficient by this turbulence model is closest to the measured value. An in-depth analysis of the flow field has been performed to understand the drag reduction mechanisms of those devices and the main findings are:

The most effective drag reduction device is the roof deflector and its major drag reduction mechanism lies in the elimination of a high pressure region on the top part of the front face of the trailer. This is because the roof deflector on top of the tractor prevents the direct impingement of flow onto the top part of the front face of the trailer. In addition, the amount of flow entering the gap region from top is also reduced due to the deployment of the roof deflector, which reduces flow interactions in the gap region, leading to less turbulence and hence less drag. Nevertheless the amount of drag reduced by this mechanism (reducing turbulence in the gap region) is much less than due to the elimination of the high pressure region on top of the front face of the trailer.

The side extenders mounted to the sides of the tractor work in a similar way as the roof deflector does, i.e., elimination of high pressure in two small narrow vertical regions on the front face of trailer and also reduction of the amount of flow entering the gap region from both sides. Since those two vertical narrow regions are much smaller than the high pressure region on the top part of the front face of the trailer so that the amount of drag reduction obtained is also much smaller. Flow interactions in the gap region are further reduced as less flow entering into the gap region from both sides.

The primary reason of drag reduction when CVTD is mounted on the front face of the trailer is due to the reduction of turbulence level since CVTD stabilizes the vortices formed within the gap region and reduces the interactions of the flow further. Nevertheless, it is worth pointing out that the amount of drag reduction achieved by reducing the turbulence level in the gap region is limited and the major reduction can be achieved by eliminating the high pressure regions on the front face of the trailer.

Author Contributions

Z. Yang planned and initiated the project, and suggested the simulations; T. Charles conducted the numerical simulations and processed the data; Y. Lu provided help in conducting the simulations. The manuscript was written through the contribution of all authors. All authors discussed the results, reviewed and approved the final version of the manuscript

Acknowledgements

Conflict of Interest

The authors declare no potential conflicts of interest with respect to the research, authorship and publication of this article.

Funding

Nomenclature

CVTD	Cross Vortex Trap Device	$\bar{U}_i$	Mean velocity component (i = 1, 2, 3)
DNS	Direct Numerical Simulation	x_i	Spatial coordinate (i = 1, 2, 3)
k-ε	k-ε turbulence model	ρ	Fluid density
LES	Large Eddy Simulation	u_i'	Fluctuating velocity component (i = 1, 2, 3)
RANS	Reynold Averaged Navier-Stokes	b	Trailer height or width
RSM	Reynolds Stress Model	g	Gap between tractor and trailer
SST k-ω	Shear Stress Transport k-ω turbulence model	C_d	Drag coefficient
		ΔC_d	Change of drag coefficient

References

[1] Bearman, P., Bluff Body Flow Research with Application to Road Vehicles, In: Browand, F., McCallen, R., Ross, J., (eds) *The Aerodynamics of Heavy Vehicles II: Trucks, buses and trains*. Springer, 41, 2009, 3-13.

[2] Abikan, A., Yang, Z., Lu, Y., Computational Analysis of Turbulent Flow over a Bluff Body with Drag Reduction Devices, *Journal of Applied and Computational Mech*anics, 6(SI), 2020, 1210-1219.

[3] Bradley, R., Technology Roadmap for the 21st-Century Truck Program, *Report for the US Department of Energy*, Washington DC, Report no. 21CT-001, 2000.

[4] Charles, T., Lu, Y., Yang, Z., Impacts of the Gap Size between Two Bluff Bodies on the Flow Field Within the Gap, *Proceedings of the 13th International Conference in Heat Transfer, Fluid Mechanics and Thermodynamics*, Portorož, Slovenia, 132-135, 2017.

[5] Charles, T., Yang, Z., Lu, Y., Numerical Analysis of Flow in the Gap between a Simplified Tractor-Trailer Model with Cross Vortex Trap Device. *International Journal of Mechanical and Mechatronics Engineering*, 13(11), 2019, 707-711.

[6] Hjelm, L., Bergqvist, B., European Truck Aerodynamics – A Comparison Between Conventional and CoE Truck Aerodynamics and a Look into Future Trends and Possibilities. In: Browand, F., McCallen, R., Ross, J., (eds) *The Aerodynamics of Heavy Vehicles II: Trucks, buses, and trains*, Springer, 41, 2009, 469-477.

[7] Yang, Z., Large-Eddy Simulation: A Glance at the Past, a Gaze at the Present and a glimpse at the Future, *the 5th International Symposium on Jet Propulsion and Power Engineering*, Beijing, China, 2014-ISJPPE-0010, 2014.

[8] Worth, N., Yang, Z., Simulation of an Impinging Jet in a Crossflow Using a Reynolds Stress Transport Model, *International Journal for Numerical Methods in Fluids*, 52, 2006, 199-211.

[9] Ostheimer, D., Yang, Z., A CFD Study of Twin Impinging Jets in a Cross-flow, *The Open Numerical Methods Journal*, 4, 2012, 24-34.

[10] Yang, Z., Assessment of Unsteady-RANS Approach against Steady-RANS Approach for Predicting Twin Impinging Jets in a Cross-flow, *Cogent Engineering*, 1, 2014, 936995.

[11] Daly, B.J., Harlow, F.H., Transport Equations in Turbulence, *Physics of Fluids*, 13, 1970, 2634-2649.

[12] Gibson, M.M., Launder, B.E., Ground Effects on Pressure Fluctuations in the Atmospheric Boundary Layer, *Journal of Fluid Mechanics*, 86, 1978, 491–511.

[13] Allan, J., Aerodynamics drag and pressure measurements on a simplified tractor-trailer model, *Journal of Wind Engineering & Industrial Aerodynamics.*, 9, 1981, 125-136.

ORCID iD

Terrance Charles https://orcid.org/0000-0002-1159-4532
Zhiyin Yang https://orcid.org/0000-0002-6629-1360
Yiling Lu https://orcid.org/0000-0001-6084-5425